Electronics Research Laboratory
University of California
Berkeley, California

COMPUTED CHARACTERISTICS OF VARIOUS MODEL CAVITY-CHAIN BEAM AMPLIFIERS[+]

by

R. M. Bevensee

This work was supported in part by the
Air Force Office of Scientific Research; Department of the Army,
Army Research Office; and Department of the Navy, Office of
Naval Research, under Grant No. AF-AFOSR-62-340

January 2, 1963

[+]Often called "extended interaction" klystrons. This report is based on Chapter 10 of the book Electromagnetic Slow Wave Systems, by R. M. Bevensee (New York: John Wiley and Sons).

1. Introduction

The microwave cavity-chain beam amplifier to be discussed is depicted in Figure 1. It is basically a traveling-wave tube with provision for stagger-tuning the various cavities in order to widen the bandwidth, which is inherently narrow because the passband of the infinitely-long, periodic structure is narrow. Generator current I_g excites the beam in the first cavity after it has entered unmodulated. The beam, assumed longitudinally-confined, traverses the various cavities and interacts with the axial electric field of each. The intermediate cavities may or may not be loaded externally; only the last cavity must be coupled to a passive load. Note there are no field-free drift spaces between cavities as in the conventional multi-cavity klystron. In this report we discuss only 5- and 10-cavity tubes.

We first develop, in Section 2, the basic equations which describe the excitation of the cavity fields by the beam and by the fields of the neighboring cavities through the coupling holes. We shall also develop the equations for the beam as driven by the electric field in each cavity and by its own space-charge field. The assumptions in the analysis are tabulated. In Section 3 we obtain the relations among all the parameters of a stagger-tuned chain in terms of the coupling-hole parameter of one cavity and the various resonant frequencies of the cavities. These may be adjusted either by external susceptive loading or by collars on the outer circumferences of the cavities. If collars are used certain of the coupling parameters must be readjusted slightly from their theoretical values in order to guarantee conservation of power throughout the amplifier. The expression for input impedance is derived.

In Section 4 we present computed characteristics of the gain and input impedance vs. frequency of several model amplifiers with zero electromagnetic coupling between cavities and lossless intermediate cavities. The output cavity is loaded to a Q_L of 50. All cavities are synchronously tuned. We find these amplifiers have tremendous gains and gain-bandwidth products but virtually no bandwidths. Their input

resistances are positive at all frequencies. The effect of adding loss to the intermediate cavities is a large reduction in gain and a slight increase in bandwidth. Computed performances of these tubes are compatible with the experimental results of M. Chodorow and T. Wessel-Berg and of H. Golde.

In Section 5 we study the effect of introducing electromagnetic coupling between cavities and matching the output cavity to the growing wave at the $3\pi/4$ "cold" circuit phase shift frequency. Invariably the coupling causes the gain to fall sharply without a significant increase in operating bandwidth. The input resistance often goes negative in certain frequency ranges. If the generator resistance is not sufficiently positive the amplifier may exhibit "cut off" oscillations at a frequency near the π-cutoff frequency.

In Section 6 we describe some models of stagger-tuned amplifiers with either zero or very slight electromagnetic coupling between cavities. If coupling is present the output cavity is matched as described in Section 5. In the absence of this coupling the stagger-tuned gains are relatively low and the gain vs. frequency curves are jagged so that the bandwidth is not increased. It appears there is no stagger-tuning scheme which will increase the bandwidth by a reasonable amount, considering the reduction of gain in such an amplifier. Then we consider various stagger-tuned arrangements of the same tube but with very light electromagnetic coupling between cavities and with the last cavity matched. The gains are negative, implying negative input resistance, so that these potentially unstable tubes are inherently narrowband even though the input resistance may be only a few ohms negative in the frequency range of interest. It is possible to taper the resonant frequencies of a tube so as to eliminate the large negative input resistance near the π-cutoff frequency. However, in the tube described herein, even a larger magnitude of negative input resistance developed near the center of the passband and the untapered tube.

The computations enable us to specify, in Section 7, characteristics of a model amplifier with both high gain and reasonable bandwidth.

The amplifiers described in this report have very low bandwidths primarily because the beam-circuit coupling coefficient is low and a final drift space is not utilized; if these amplifiers are used as bunchers, and the output kinetic voltage is allowed to drift into current which excites the (broadband) output cavity, then performance is markedly improved (Section 7). Electromagnetic coupling between the buncher cavities and/or the proper stagger-tuning of those cavities can improve the overall performance. Drift spaces between the buncher cavities are not crucial, although they undoubtedly would help to optimize the performance. Conventional 5- and 7-cavity klystrons (with drift spaces but no coupling between cavities) have gains in the range 20-30 db and bandwidths of 5-10%. Our computations are compatible with these numbers, provided the output cavity is optimized with respect to both gain and bandwidth and also the (ω/ω_q) ratio is maintained high.

2. Assumptions and Equations of the Analysis.

In the amplifier of Figure 1 the beam enters the first cavity unmodulated and is longitudinally confined by a large axial magnetic field. The cavities are considered lossless (see remarks under assumption (4)), of a common length L, and tuned either by an external susceptive load or by high-Q metal collars. No field-free drift spaces lie between successive cavities although the beam equations could easily be modified to include them. The ac magnetic field in the last cavity induces current I_L to flow to the external load. The fields in each cavity are excited by the beam, by the fields in neighboring cavities if the net electromagnetic coupling is finite, and by the loop currents.

We will discuss the small-signal ac power gain and input impedance as functions of frequency for various output loads and cavity parameters with the following assumptions:

(1) There is only loop coupling via coaxial lines to the external loads.

(2) The longitudinal beam excitations are represented by the usual fast and slow space-charge mode expressions for kinetic voltage and current.

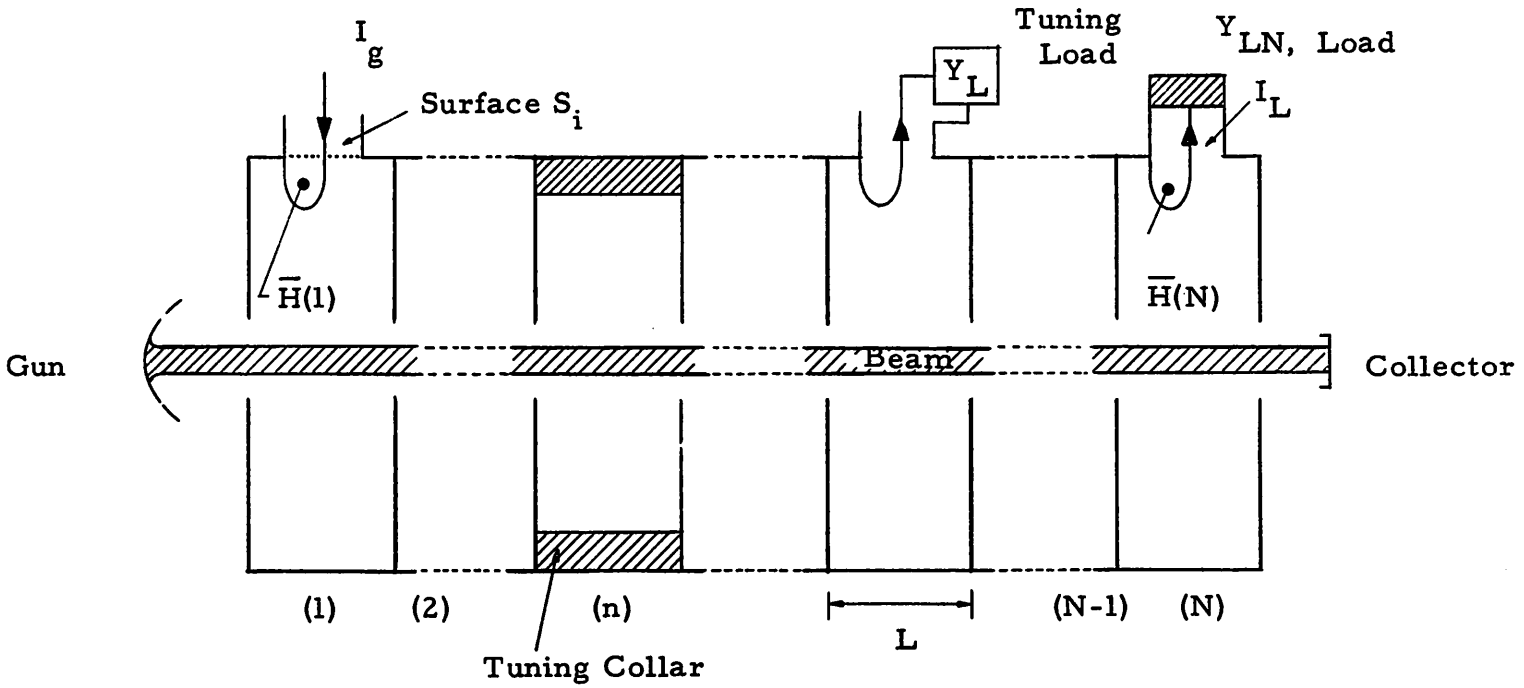

Figure 1. The Cavity-chain Beam Amplifier. The Cavities are Stacked Next to Each Other.

We do not account for non-linear effects even if the gain is considerable.

(3) We represent the fields of each cavity by the two modes which resonate when the coupling holes are covered by perfect electric and perfect magnetic shorts, respectively. The first mode represents the true fields at zero phase shift per cavity in an infinitely long chain; the second mode represents the true fields at π phase shift. The operating frequency always lies near the resonant frequencies of these two modes, so that we can neglect the other weakly-excited modes. This assumption implies that the first pass band of the infinitely-long, unstaggered chain of cavities is narrow compared to the width of the passband between the first and second pass bands.

(4) The intermediate cavities are assumed to be lossless unless otherwise specified. This assumption is reasonable if the cavities have unloaded Q's of about 10^4 or more. If the external conductive loading of these cavities is gradually increased the gain at first drops very rapidly, then less and less rapidly, while the bandwidth increases slowly if at all. This external loading improved none of the amplifiers summarized in Sections 4-6 to the extend of making the bandwidth > 1%.

(5) The dimensions of each cavity are uniform except perhaps for the outer radius which may be varied by means of a collar to change the resonant frequencies of both the "short" circuit mode (resonating between electrically-shorted holes) and the "open"-circuit mode (resonating between magnetically-shorted holes). Alternatively, the cavities are tuned externally.

(6) The cavity length L is presumed to be about three times the center hole diameter so that the axial electric field within that cavity is nearly uniform across the cavity. Figure 2 shows the $\bar{e}_z$-field pattern in the beam region. The amplitude of this pattern is, of course, determined by the beam current and fields on the center holes. This important assumption enables us to say that the $\bar{e}_z$-pattern is essentially independent of operating frequency.

(7) We assume a thin solid or hollow beam and neglect the radial variation of $\bar{e}_z$ in any given transverse cross section. We take the

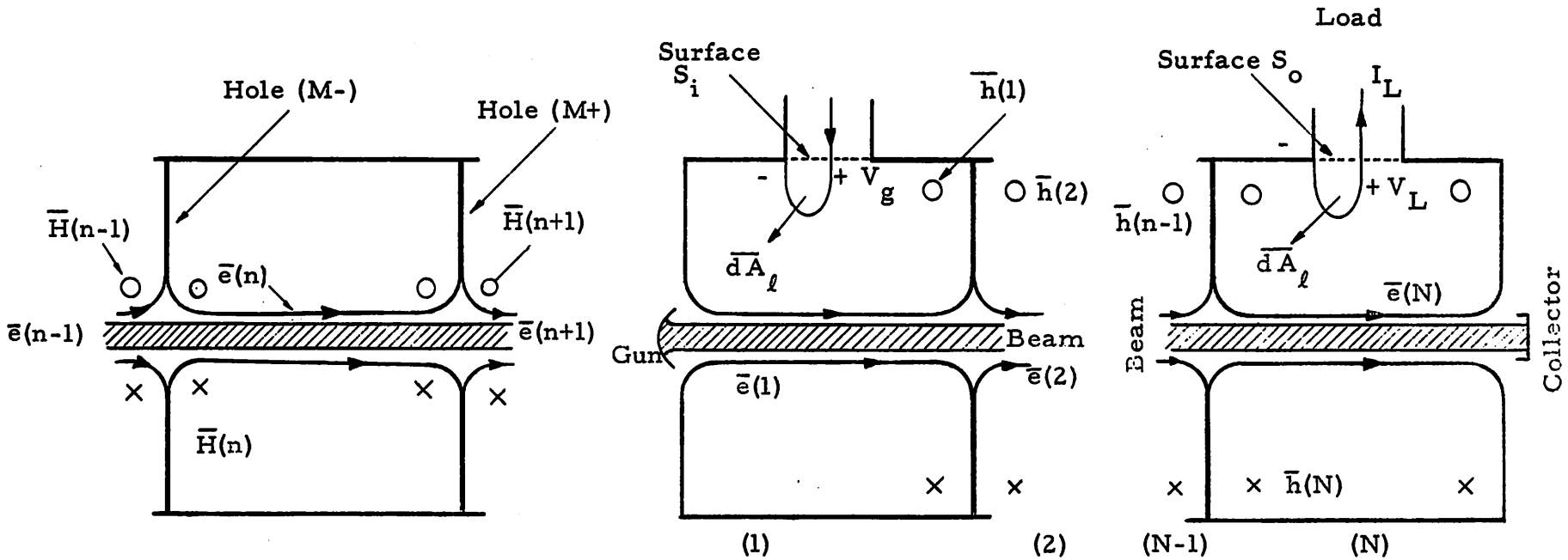

(a) Intermediate Cavity (n). (External loading not shown.)

(b) Input Cavity (1).

(c) Output Cavity (N).

Figure 2. The Individual Cavities in the Chain.

space-charge reduction factor ω_q/ω_p to be constant throughout the amplifier. The space-charge electric field is taken to be proportional to the ac beam current by the usual space-charge-mode factor $jZ_o\omega_q/u_o$, Z_o being the ac beam impedance per unit area and u_o, the dc beam velocity.

(8) We neglect the fringing of the electric field near each centerhole and simply say the axial electric field of one cavity acts upon the beam right up to one centerhole, just beyond which the field of the next cavity "takes over" and drives the beam further. This assumption is reasonable because the cavities are long compared to the centerhole diameter which measures the fringing-field region. The assumption does <u>not</u> imply any discontinuity in power flow across each centerhole if the neighboring cavities are not stagger-tuned; if they are stagger-tuned there is a slight discrepancy between the estimated electromagnetic coefficients at the common centerhole and the values chosen to maintain continuity of electromagnetic power flow. Details of this statement will be discussed later in this section.

(9) To keep the analysis as realistic as possible we work with Maxwell's equations directly and do not introduce equivalent circuit elements except for the input and output impedances, both of which are well-defined in the coaxial waveguides.

Granted that these assumptions are reasonable for a good description of the cavity-chain amplifier we shall now summarize the equations for the fields and beam excitations in each cavity.

It is convenient to represent the solenoidal fields in the n^{th} cavity $(1 \leq n \leq N)$ with the open-circuit mode defined earlier. The field pattern $\bar{e}(n)$ and $\bar{h}(n)$ of this mode, which represents the two fields at π phase shift per cavity in a periodic chain, are defined conveniently as

$$\nabla \times \bar{e}(n) = p(n)\,\bar{h}(n) \qquad \bar{e}(n)\cdot\bar{n} = 0 \quad \text{on holes} \tag{1a}$$

$$\nabla \times \bar{h}(n) = p(n)\,\bar{e}(n) \qquad \bar{h}(\bar{n}) \times \bar{n} = 0 \quad \text{on holes} \tag{1b}$$

$p(n)$ is the normalized resonant frequency of this mode. We let these

patterns have amplitudes v(n) and i(n), respectively. Maxwell's equations modified for the presence of the beam then are

$$\nabla \times \left[v(n)\,\bar{e}(n)\right] = -\,j\omega\mu\, i(n)\,\bar{h}(n) \tag{2a}$$

$$\nabla \times \left[i(n)\,\bar{h}(n)\right] = J + j\omega\epsilon\, v(n)\,\bar{e}(n) \tag{2b}$$

When we operate on these equations so as to obtain v(n) and i(n) by a procedure described by Schelkunoff[1] we obtain:

$$p(n)\, v(n) = -j\omega\mu\, i(n) \tag{3a}$$

$$p(n)\, i(n) = \frac{1}{\tau(n)} \int_{\text{holes}} \bar{e}(n) \times H \cdot \bar{n}\, ds + \frac{1}{\tau(n)} \int_{V} J \cdot \bar{e}(n)\, dv + j\omega\epsilon\, v(n) \tag{3b}$$

Here $\tau(n)$ is the volume of the n^{th} cavity to which the field patterns have been normalized.

$$\int_{\text{cav}(n)} \bar{e}(n)^2\, dv = \int_{\text{cav}(n)} \bar{h}(n)^2\, dv = \tau(n) \tag{4}$$

$\bar{n}$ is the unit outward normal on the centerholes on which the magnetic field is H, and J is the beam current density in the cavity. H is given very accurately by the average of the solenoidal short-circuit mode expressions for it on either side. For example, on hole (M-) in Figure 2a, we have

$$H_{\tan}(M-) = \frac{1}{2}\left[I(n-1)\,\bar{H}(n-1) + I(n)\,\bar{H}(n)\right] \tag{5}$$

for which we use the short-circuit mode of field patterns defined by analogy with Eq. 1 as

[1] S. A. Schelkunoff, "Representation of Electromagnetic Fields in Cavities in Terms of Natural Modes of Oscillation," Journal Applied Physics, 26, 1233, October 1955.

$$\nabla \times \overline{E}(n) = P(n)\,\overline{H}(n) \qquad \overline{E}(n) \times \overline{n} = 0 \quad \text{on holes} \tag{6a}$$

$$\nabla \times \overline{H}(n) = P(n)\,\overline{E}(n) \qquad \overline{H}(n) \cdot \overline{n} = 0 \quad \text{on holes} \tag{6b}$$

P(n) is the normalized resonant frequency of this mode. The amplitudes of the electric and magnetic fields as given by this mode are V(n) and I(n); for consistency with the fields as expressed by the open-circuit mode in Eq. 2 we must take $I(n) \equiv i(n)$.

A complete discussion of the use of these solenoidal and the associated irrotational modes for expanding fields in cavities is given in the reference [2].

By eliminating i(n) from Eq. 3 and with relation 5 we obtain the basic equation for v(n) of an intermediate cavity $(n \neq 1, N)$ as

$$\left[p(n)^2 - k^2 + \frac{p(n)}{\tau(n)} \int_{M-} \overline{e}(n) \times \overline{H}(n) \cdot \overline{i}_z \, ds\right] v(n) + \frac{p(n-1)\,v(n-1)}{2\,\tau(n)} \cdot$$

$$\int_{M-} \overline{e}(n) \times \overline{H}(n-1) \cdot \overline{i}_z \, ds - \frac{p(n+1)\,v(n+1)}{2\,\tau(n)} \int_{M+} \overline{e}(n) \times \overline{H}(n+1) \cdot \tag{7}$$

$$(k^2 = \omega^2 \mu\epsilon).$$

$$\cdot \overline{i}_z \, ds + \frac{j\omega\mu}{\tau(n)} \int_V J \cdot \overline{e}(n) \, dv = 0$$

If the intermediate cavity is loop-coupled to an external load an additional term appears, according to the discussion of the last cavity. For the first or input cavity we must modify Eq. 7 as follows. We discard the v(n - 1) term (with n = 1 now) because no cavity is present on the gun side. And we must add a loop-excitation term to the right side of Eq. 7,

[2] R. M. Bevensee, "Periodic Electromagnetic and Quantum Systems," Annals of Physics, 12, No. 2, pp. 222-263, Feb., 1961.

derived as follows. The loop term on the left side is, by analogy with the beam term,

$$\left[j\omega\mu/\tau(1)\right] I_g \int_{\text{loop}} \overline{d\ell} \cdot \overline{e}(1)$$

From $\nabla x\, \overline{e}(1) = p(1)\, \overline{h}(1)$ we can write

$$\oint_{\text{loop}} \overline{e}(1) \cdot \overline{d\ell} = -\int_{\text{loop}} \nabla x\, \overline{e}(1) \cdot \overline{dA_\ell} = -p(1) \int \overline{h}(1) \cdot \overline{dA_\ell}$$

$$\simeq -p(1) \left|\overline{h}(1)\right|_{\text{loop}} \cdot A_{\ell 1} \tag{8}$$

$A_{\ell 1}$ being the loop area inside surface S_i of Figure 2b. These expressions will imply continuity of power flow across the input surface S_i. Thus, Eq. 7 for the input cavity will have the following term on the right side:

$$+\frac{j\omega\mu}{\tau(1)} I_g\, p(1) \left|\overline{h}(1)\right|_{\text{loop}} \cdot A_{\ell 1} \tag{9}$$

For the last cavity N, the output cavity, we must modify Eq. 7 as follows. We drop the $v(N+1)$-term because there is no cavity on the collector side of cavity N. Tangential electric field on coupling surface S_o in Figure 2c does not excite the cavity mode because the former is asymmetric with respect to $\overline{h}(N) = \overline{h}_\theta(N)$. The loop excitation of the cavity is, by analogy to the beam term,

$$\left[j\omega\mu/\tau(N)\right] I_L \oint_{\text{loop}} \overline{dl} \cdot \overline{e}(N) = \frac{j\omega\mu}{\tau(N)} I_L\, p(N) \left|\overline{h}(N)\right|_{\text{loop}} A_{\ell N} \tag{10}$$

Loop current I_L can be related to the external load Y_L measured on surface S_o as $I_L = V_L Y_L$. Lastly, V_L is given by Faraday's law for the loop,

$$V_L = \oint_{loop} e \cdot \overline{d\ell} = v(N)\, p(N)\, |\bar{h}(N)|_{loop} A_{\ell N} \qquad (11)$$

All these statements tell us that Eq. 7 for last cavity (N) will add the following term to the left side,

$$+ \frac{j\omega\mu}{\tau(N)} Y_L \left[p(N)\, |\bar{h}(N)|_{loop} A_{\ell N} \right]^2 v(N) \qquad (12)$$

We now know the expression for the amplitude of the solenoidal electric field, v(n), in each cavity, as "driven" by beam current density J. The irrotational axial electric field in the beam region will be represented by $jZ_o(\omega_q/u_o)\,J$, as mentioned earlier. We now must solve the longitudinal beam equations for J and kinetic voltage V_k in each cavity,

$$(j\beta_e + \partial/\partial z)\, V_k(z) = v\bar{e}_z + j z_o \beta_q J(z) \qquad (13a)$$

$$(j\beta_e + \partial/\partial z)\, J(z) = j Y_o \beta_q V_k(z) \qquad (13b)$$

with

$$\beta_e = \omega/u_o, \quad \beta_q = \omega_q/u_o \qquad (13c)$$

$$Y_o = \frac{1}{2} \frac{|J_o|}{V_o} \frac{\omega}{\omega_q}, \quad V_o \text{ being the beam voltage.}^{+}$$

Suffice it to say that these equations may be solved for $V_K(n+1)$ and $J(n+1)$ leaving the n^{th} cavity in terms of $V_K(n)$ and $J(n)$ entering the cavity and v(n), $\bar{e}_z$ being uniform across the cavity. The results may be cast into the form

$$V_K(n+1) = A_1 V_K(n) + A_2 J(n) + A_3 v(n) \qquad (14a)$$

$$J(n+1) = B_1 V_K(n) + B_2 J(n) + B_3 v(n) \qquad (14b)$$

+A relativistic correction factor divides Z_o and multiplies Y_o according to the appendix of Reference 2. This becomes more important at higher beam voltages above 50 kv.

The A_i- and B_i- coefficients are functions of $\beta_e L$, $\beta_q L$, k, and the other cavity parameters.

We can also obtain J(z) in each cavity n by solving Eq. (13b) in terms of $V_K(n)$, J(n), and v(n). Then we can integrate J(z) for Eq. 7 and obtain an expression for v(n) in terms of $V_K(n)$ and J(n). This latter expression along with Eq. 14 furnish a set of 3 equations for each cavity. It is convenient to cast these 3 equations into forms which involve the following convenient normalized parameters:

$\phi(n) = v(n)L$, the "voltage" for cavity n.

$I_b(n) = Z_o J(n)$, the beam current density in volts.

$\pi_n = P(n)/P_r$, the normalized short-circuit mode resonant frequency in cavity n. P_r is any convenient reference frequency (in units of $k = \omega\sqrt{\mu\epsilon}$).

$\rho_n = p(n)/P_r$, the normalized open-circuit mode resonant frequency.

$\mathcal{K} = k/P_r$, normalized operating frequency.

$$m_{nn} = +\frac{1}{P_r \tau(n)} \int_{M-} \bar{e}(n) \times \bar{H}(n) \cdot \bar{i}_z \, ds = -\frac{1}{P_r \tau(n)} \int_{M+} \bar{e}(n) \times \bar{H}(n) \cdot \bar{i}_z \, ds, < 0,$$

the normalized self-coupling coefficient of cavity n.

$$m_{n,n+1} = \frac{1}{P_r \tau(n+1)} \int_{M+} \bar{e}(n+1) \times \bar{H}(n) \cdot \bar{i}_z \, ds, < 0,$$

a normalized cross-coupling coefficient.

$$m_{n+1,n} = \frac{-1}{P_r \tau(n)} \int_{M+} \bar{e}(n) \times \bar{H}(n+1) \cdot \bar{i}_z \, ds < 0,$$

another cross-coupling coefficient.

$$D = p(1) \left|\bar{h}(1)\right|_{\text{loop}} A_{\ell 1} / \left[P_r^2 \tau(1)\right],$$

the loop parameter.

$I_G = \omega\mu I_g L$, normalized input loop current.

$Y_{Ln} = \frac{\omega\mu}{\tau(n)} \left(\frac{p(n) \left| \bar{h}(n) \right|_{loop} A_{\ell n}}{P_r} \right)^2 Y_L$, normalized load admittance.

In terms of these variables the complete set of equations for the cavity-chain beam tube is given in Table 1. C_B is a parameter which measures the coupling between the beam and circuit field; it is given by

$$C_B^2 = \frac{\omega\mu e_z^2 A_b Y_o}{P_r^2 \beta_e^2 \tau} \simeq \frac{\omega\mu e_z^2}{P_r^2 \beta_e^2 \tau} \frac{1}{2} \frac{|I_o|}{V_o} \frac{\theta_e}{\theta_q}, \tag{16}$$

A_b being the beam area. There are 3N-2 equations in terms of the 3N-2 variables $\phi(n)$, $V_K(n)$, and $I_b(n)$, excluding $V_K(1)$ and $I_b(1)$ entering the first cavity, which are zero.

3. Relationships Among the Parameters

If we wish to stagger-tune the various cavities with external susceptive loading, the expression for a_{nn} in Table 10-1 shows that the effective normalized resonant frequency ρ_n' differs from the non-loaded ρ_n by

$$(\rho_n')^2 = \rho_n^2 - B_{Ln} \qquad B_{Ln}, \text{ normalized susceptive load.} \tag{17}$$

Thus a capacitive load lowers the effective resonant frequency. On the other hand we may wish to stagger-tune by staggering the radii $R_1, \ldots, R_N$ of the various cavities. In this section we shall develop the relations between the parameters of different cavities in such a chain in terms of the ratios of their normalized short-circuit mode resonant frequencies.

Since the short-circuit mode resonates in the n^{th} cavity such that $J_o \left[P(n) R_n \right] = 0$, J_o being the Bessel function, we have $P(n+1)/P(n) = \pi_{n+1}/\pi_n = R_n/R_{n+1}$

To obtain relations among the m's we first observe the short-circuit mode patterns in the n^{th} cavity near the small centerholes are

$$\bar{E}(n) = \bar{i}_z \sqrt{3.71}\ J_o\left[P(n)\, r\right] \simeq \bar{i}_z\, 1.93 \qquad r << R_n \tag{18a}$$

$$\bar{H}(n) = \bar{i}_\theta \sqrt{3.71}\ J_1\left[P(n)\, r\right] \simeq \bar{i}_\theta\, 1.93\, P(n)\, r/2 \tag{18b}$$

The factor $\sqrt{3.71}$ normalizes the mode pattern just as $\bar{e}(n)$ and $\bar{h}(n)$ are normalized by Eq. 4. We see that $\bar{H}_\theta(n+1) / \bar{H}_\theta(n)$ at a point on the hole between cavity n and cavity $(n+1)$ is $P(n+1)/P(n) = \pi_{n+1}/\pi_n$. Now, the open-circuit mode pattern $\bar{e}(n)$ is a perturbation of the nearly-uniform $\bar{E}(n)$-pattern near the holes, thus: $|\bar{e}(n)| = |\bar{e}(n+1)| = |\bar{e}(n+2)| = \ldots$ at the same transverse point on the various holes. From the definition of m_{nn} in Eq. 15 and the fact that $\tau(n)$ varies only with radius R_n as $\tau(n+1)/\tau(n) = (\pi_n/\tau_{n+1})^2$ we find that

$$m_{n+1,\,n+1} = (\pi_{n+1}/\pi_n)^3\, m_{nn} \tag{19}$$

From the definitions of the other two m's we learn they are related as

$$m_{n,\,n+1} = (\pi_{n+1}/\pi_n)^2\, m_{nn} \tag{20a}$$

$$m_{n+1,\,n} = (\pi_{n+1}/\pi_n)\, m_{nn} \tag{20b}$$

Therefore a choice of all the radii R_n will determine all the normalized short-circuit mode frequencies π_n and all the coupling coefficients m_{ij} in terms of just one of the m_{nn}. Any one of these is determined by the (fixed) size of the centerholes and R_n.

We now must ascertain the open-circuit mode normalized frequency ρ_n. It is related to π_n and m_{nn} through Green's theorem,

$$\int_V (\overline{A} \cdot \nabla \times \nabla \times \overline{B} - \overline{B} \cdot \nabla \times \nabla \times \overline{A}) \, dv = \oint_S (\overline{B} \times \nabla \times \overline{A} - \overline{A} \times \nabla \times \overline{B}) \cdot \overline{d}s \tag{21}$$

By substituting $\overline{A} = \overline{e}(n)$ and $\overline{B} = \overline{E}(n)$ we obtain, with the mode relations of Eq. 1 and corresponding ones for $\overline{E}(n)$ and $\overline{H}(n)$,

$$\left[P^2(n) - p^2(n)\right] \int_V \overline{E}(n) \cdot \overline{e}(n) \, dv = 2P(n) \int_{M-} \overline{e}(n) \times \overline{H}(n) \cdot \overline{i}_z \, ds \tag{22}$$

For small centerholes, $\int_V \overline{E}(n) \cdot \overline{e}(n) \, dv \simeq \tau(n)$, the cavity volume to which each pattern is normalized. With $P(n) \simeq p(n)$ we obtain, approximately,

$$P(n) - p(n) = \frac{1}{\tau(n)} \int_{M-} \overline{e}(n) \times \overline{H}(n) \cdot \overline{i}_z \, ds \tag{23a}$$

and upon dividing by reference frequency P_r we have

$$\pi_n - \rho_n = m_{nn} \tag{23b}$$

This relation determines each ρ_n after the π_n's and m_{nn}'s have been specified.

The foregoing relations determine all the cavity parameters in terms of just one m_{nn} and all the radii R_n. Unfortunately the relations for $m_{n,n+1}$ and $m_{n+1,n}$ are not quite right to guarantee conservation of electromagnetic power flow across each hole of a stagger-tuned chain ! With Eq. 5 the power flow out of cavity n into cavity (n + 1) is

$$P_{av} = \frac{1}{2} \text{ Real} \int_{M+} v(n) \, \overline{e}(n) \times \frac{1}{2} \left[I^*(n) \, \overline{H}(n) + I^*(n+1) \cdot \right.$$

$$\left. \cdot \overline{H}(n+1) \right] \cdot \overline{i}_z \, ds, \tag{24a}$$

which, with the relation $pv = -j\omega\mu i$ for each cavity, and $i = I$, is just

$$P_{av} = \frac{1}{4} \text{ Real } \frac{v(n)\, p(n+1)\, v(n+1)^*}{j\omega\mu} \int_{M+} \bar{e}(n) \times \bar{H}(n+1) \cdot \bar{i}_z \, ds \qquad (24b)$$

Likewise the power flowing into cavity $(n + 1)$ can be expressed as

$$P_{av} = \frac{1}{4} \text{ Real } \frac{v(n+1)\, p(n)\, v(n)^*}{j\omega\mu} \int_{M+} \bar{e}(n+1) \times \bar{H}(n) \cdot \bar{i}_z \, ds \qquad (25)$$

Upon conjugating this expression we see it will only equal the preceding one if

$$p(n+1)\, \tau(n)\, m_{n+1,\,n} = p(n)\, \tau(n+1)\, m_{n,\,n+1} \qquad (26a)$$

i.e., if

$$\frac{\rho_{n+1}}{\rho_n} \left(\frac{\pi_{n+1}}{\pi_n} \right)^2 m_{n+1,\,n} = m_{n,\,n+1} \qquad (26b)$$

This last relation is somewhat incompatible with the preceding equations, and so we must readjust each $m_{n,n+1}$ and $m_{n+1,n}$ slightly in order to guarantee Eq.26 and therefore continuity of power flow. There is no unique way to do this; we have changed one about as much as the other for the computations.

Our description of the cavity fields is therefore not perfect, and the ambiguity in these coupling coefficients is greater for a greater disparity in resonant frequencies of cavities n and $(n + 1)$. However, the small errors in the computed power gains and input impedances would not change our conclusions about the amplifiers we shall describe in later sections of this report.

We have included in the computer program a power-check computation, whereby the power flowing into the first cavity may be compared

to the load power and beam power leaving the last cavity. By means of this computation we are certain the errors in the computed gains of various amplifiers are negligible.

The input impedance of the amplifier is given, with the aid of Eq. 8, by

$$Z_{in} = V_g/I_g = \oint_{loop} \bar{e}(1) \cdot \overline{d\ell}/I_g = \phi(1)\, p(1)\, |\bar{h}(1)|_{loop} A_{\ell 1}/(I_g L)$$

$$= \phi(1)\; p(1)\, |\bar{h}(1)|_{\ell} A_{\ell 1}\, \omega\mu\, /I_G \qquad (27)$$

To know the constant of proportionality between Z_{in} and $\phi(1)$ we must know both loop and cavity parameters. A particular tube of interest had the parameters $\omega = 2\pi(3\ \text{kmc})$, $|\bar{h}|_{loop} = 1$, loop diameter 1 cm, $\tau \simeq 10^{-4}\ m^3$, and $L \simeq 0.7''$. We chose $I_G \equiv p(1)\, |\bar{h}(1)|_{loop} \cdot A_{\ell 1}\omega\mu$ so that $Z_{in} \equiv \phi(1)$. Then it follows that the loop excitation parameter DI_G in Table 1 is 0.48.

All of the computed results in this report are for this value of DI_G, such that $Z_{in} \equiv \phi(1)$ for this reference tube.

4. Performance Characteristics of Model 10-Cavity Power Amplifiers, Synchronously-Tuned and with no Electromagnetic Coupling Between Cavities

In this section we shall tabulate the frequency response characteristics of typical model 10-cavity tubes with the parameters $\theta_e = \omega L/u_o = 2.24$ and $\theta_q = \omega_q L/u_o = .235$, for various values of beam-circuit coupling coefficient, C_B. Reasons for this choice of θ_e and θ_q are given in the next section. The output cavity is loaded to a Q_L of 50 without the beam and the high-Q intermediates are treated as lossless. Zero electromagnetic coupling between cavities

can be effected by cutting slots or holes into the outer portions of the partitions between cavities so as to cancel the centerhole coupling.

The gain and input impedance characteristics of three such amplifiers with the practical C_B-values of .028, .0707, and .100 are tabulated in Tables 2-4. The gain G is defined as

$$G = \frac{\text{load power}}{\text{power into first cavity}} \tag{28}$$

and is negative if the input resistance is negative. G is distinguished from the transducer gain G_T defined as

$$G_T = \frac{\text{load power}}{\text{available source power}} \tag{29}$$

The relation between these two gains is

$$G_T = |G| \frac{4 R_g |R_{in}|}{(R_g + R_{in})^2}, \quad R_g + R_{in} > 0 \tag{30}$$

where R_g is the generator resistance. The generator reactance is chosen to cancel the tube reactance in the definition of G_T.

The fact that

$$Q_L = (k/P_r)^2 / G_{Ln} \simeq 1/G_{Ln} \tag{31}$$

in terms of the normalized load $Y_{Ln} = G_{Ln} + jB_{Ln}$ may be verified from the expression for load $P_L = 1/2 \text{ Re } Y_L |V_L|^2$, V_L given by Eq. 11, together with the expression for Q,

$$Q_L = \frac{\omega W_s}{P_L} = \omega \frac{1}{2} \epsilon |v(n)|^2 \tau(n)/P_L \tag{32}$$

This loaded Q_L is essentially the external Q defined without the beam since the cavity Q by itself is usually well over 10^3.

We see from the tables that input resistance R_{in} is always positive and gain G is very high at a frequency near the cutoff frequency ($\mathcal{K} = 1$) where the input impedance is on the order of hundreds of ohms. Naturally, the operating bandwidths of these tubes are virtually zero. It is perhaps surprising that the gains are so high with the cavities merely stacked together without optimized drift spaces between them.

The theoretical performances of these and similar tubes is consistent with the experimental results obtained by Chodorow and Wessel-berg[3] and by Golde[4]. Golde, in particular, obtained remarkable performance with a 5-cavity tube, each cavity being a full electronic wavelength section of ring-bar helix. He obtained a synchronous small-signal gain of 53db and a fractional bandwidth of 0.9%. By stagger-tuning the cavity resonant frequencies he raised the bandwidth to 2.0%; the gain dropped to 50db. Each of his cavities was loaded to a Q_L of 45.

In order to verify qualitatively our small-signal analysis we analyzed a model of Golde's tube with essentially the same parameters but with cavities of uniform $\bar{e}_z$-field and $\theta_e = \pi$ instead of 2π. Therefore we designed the model with ten cavities instead of five and with C_B adjusted accordingly. If the intermediate cavities are lossless the gain of the model tube was 85 db at midband and the bandwidth was 0.2%. Upon increasing the external loading of the intermediates, with

---

[3] M. Chodorow and T. Wessel-Berg, "A High-efficiency Klystron with Distributed Interaction," IRE Transactions of the PGED, 8, No. 1, p. 44, January, 1961.

[4] H. Golde, "A Stagger-tuned Five Cavity Klystron with Distributed Interaction," IRE Transactions of the PGED, 8, No. 3, p. 192, May, 1961.

the output cavity Q of 50, the gain decreased rapidly to 40 db at 0.7% bandwidth for an intermediate cavity Q of 100. We judge on the basis of these figures that an amplifier which employs the helix-type of cavities each of $\theta_e = 2\pi$ has better small-signal gain and bandwidth than does an amplifier which employs twice as many cavities, each of $\theta_e = \pi$.

5. Performance Characteristics of Model Synchronously-Tuned Tubes with Various Degrees of Electromagnetic Coupling

For these 10-cavity amplifiers we also specify $\theta_e = 2.24$ and $\theta_q = .235$, as well as various values of fractional passband width m (refer to Eq. 23b) and coupling coefficient C_B. We chose those values of θ_e and θ_q so the beam would be nearly synchronous with the $3\pi/4$-phase-shift frequency of an infinite chain, near which many tubes are operated for gain. In the range $0 < C_B \lesssim .10$ the growing wave is about optimum with respect to both rate of growth and real power flow per unit amplitude $|v|$.

First, let the electromagnetic coupling between cavities be very light: $m = -.01$, with the output cavity matched to the growing wave at the $3\pi/4$-phase-shift frequency. Table 5 presents the frequency characteristics for $C_B = .028$, and Table 6, the characteristics for $C_B = .10$. Note that these two tubes perform quite differently. The tubes with intermediate values of C_B are not particularly interesting. The effect of this small amount of electromagnetic coupling is to change the tube performance drastically from that given by Table 2 to that given by Table 5; in particular, the input resistance now goes abruptly negative in the tube of $C_B = .028$ and is wholly negative in the tube of $C_B = .10$. Thus, these tubes could only be operated for high stable gain in a very narrow frequency range about that frequency where $R_g + R_{in}$ (> 0) is a minimum.

Now let the coupling be increased so that $m = -.04$. This has a profound effect on the tube of $C_B = .028$; now its gain is only 20 or so throughout the frequency range near cutoff. For $C_B = .0707$

we have the curious characteristics listed in Table 7. There is absolutely no way to predict such performance on the basis of simple theory. Comparison with Table 3 indicates a completely different impedance behavior due to the coupling; whereas the decoupled-cavity tube should be operated at a frequency very close to cutoff with a matched generator resistance of about 100 ohms the tube of $m = -.04$ must be operated near $\beta = .986$ with a generator resistance of at least 13 ohms to prevent oscillation at other frequencies. An increase of C_B to .10 changes the performance to that of Table 8; the tendency to oscillate is somewhat increased, as expected.

If we now increase the coupling to $m = -.07$, and keep the tube matched at the $3\pi/4$-phase-shift frequency, the response is given by Table 9 for $C_B = .0707$. There is an abrupt transition from positive to negative input resistance at a frequency near the cutoff.

Lastly, we present the response of one of the tubes in the $m = -.10$ class, with $C_B = .10$, in Table 10. Unexpectedly, the effect of increasing both $|m|$ and C_B results in a minimum R_{in} of only -28 ohms, as compared to -300 ohms for the preceding tube.

The information in these tables proves that, even though the tubes are matched at the $3\pi/4$-phase-shift frequency, the input resistance can go sufficiently negative at frequencies near cutoff to allow troublesome cutoff oscillations observed in many tubes. The load required for match to the growing wave changes rapidly with frequency near the cutoff.

A few remarks about the transducer gain-fractional bandwidth (G_TFB) product may be of interest. The G_TFB of a tube with negative input resistance can be made as large as desired by making $(R_g + R_{in})$ sufficiently close to zero, whereupon the bandwidth also approaches zero. The G_TFB products for the uncoupled-cavity tubes of Tables 2-4 range from about 10^2 to 10^7. But the best tubes for both good gain and reasonable bandwidth have products at the low end of this range. The G_TFB product of Golde's tube, previously described is about 2×10^3 and the product of a 30 db tube of 10% bandwidth is 10^2.

The cavity-chain tubes with synchronously-tuned cavities and either zero or finite electromagnetic coupling tend to have huge gains and minute bandwidths. We now discuss the effects of stagger-tuning their resonant frequencies in various ways.

6. Performance Characteristics of Model Stagger-Tuned Amplifiers, Both with Zero and Finite Coupling Between Cavities

In these tubes there are no field-free drift spaces between cavities, and the intermediate cavities remain unloaded and lossless. We can summarize all the computed results as follows. If the cavities are decoupled the stagger-tuned gain is reduced considerably and the bandwidth is not increased. If they are coupled slightly the gains go negative so that the high-gain bandwidths are necessarily small.

We chose to describe the tube with the parameters $\theta_e = 2.36$, $\theta_q = 0.40$, $C_B^2 = .010$. With no electromagnetic coupling between cavities the last cavity was loaded to a Q_L of 50. With the light coupling of $m = -.01$ the last cavity was matched to the growing wave at the unstaggered $3\pi/4$-phase-shift frequency.

First, let us consider a 5-cavity tube with no coupling: $m = 0$. The unstaggered tube has a transducer gain $G_T = 44$ db, a fractional bandwidth of 0.15% and an input impedance of $132 + j51$ ohm at the center frequency. Performance for two typical stagger-tuning arrangements is summarized in Tables 11 and 12. Obviously the tube gains are low and vary erratically with frequency.

Now, when we consider various stagger-tuned arrangements of the same tube with the light coupling of $m = -.01$ and the last cavity matched as before we compute negative gains of low magnitude on the average; i.e., potentially unstable tubes. The performance of two representative stagger-tuned 10-cavity tubes is given in Tables 13 and 14, to be compared with the synchronously-tuned uncoupled tube of gain 110 db and fractional bandwidth 0.10% (output cavity $Q_L = 50$). If the stagger-tuned tubes are to be stable the generator resistance R_g

must be chosen so $(R_g + R_{in,\,min}) > 0$, in which case the high-gain-bandwidth product will be necessarily rather small.

We have verified by a particular example the fact that it is possible to avoid a large negative input resistance near the π-cutoff frequency by tapering the resonant frequencies of the cavities. To be specific, we tapered the short-circuit mode resonant frequencies of the amplifier of Table 10 from $.885\,p_5$ in the first cavity (p_5 of the fifth cavity is reference) to $.918\,p_5$ in the tenth cavity by means of collars. As open-circuit mode resonant frequencies increased monotonically from $.98\,p_5$ to $1.024\,p_5$. $m_{5,5} = -.10$ was reference, whereupon $m_{1,1} = -.095$, $m_{10,10} = -.106$ and the other m_{ij} were calculated as outlined in Section 3. The values of $m_{n,n+1}$ and $m_{n+1,n}$ were re-adjusted a few percent each to guarantee conservation of power by Eq. 26 b. The result of this tapering is a change in the minimum value of R_{in} from $\simeq -30$ ohms at relative frequency $K = .992$ to $\simeq -55$ ohms at $K = .967$. This untapered tube has a fractional passband width of about 10%. As frequency increases in the tapered tube above this value of $K\,R_{in}$ increases to about zero at $K = 1.0$. Thus, the tapering has essentially only lowered the frequency at which we must operate the tube for high gain without oscillation.

7. Remarks about the Characteristics of an Amplifier with Good Gain and Bandwidth

The computed performances of these various synchronously tuned and stagger-tuned model amplifiers with no drift spaces between cavities and low beam-circuit coupling indicate clearly that one cannot hope to obtain both reasonable gain and reasonable bandwidth in the same tube. Reasonable performance figures measured for 5- and 7-cavity tubes lie in the range of 20-30 db maximum gain and 5-10% bandwidth. For example, L. Smullin[5] reports on the behavior of

[5] L. D. Smullin and D L. Morse, "M. I.T. Quarterly Progress Report," Microwave Electronics Section, Research Laboratory of Electronics, M. I. T., January 15, 1960.

a 5-cavity multicavity klystron called a "skirtron" (Litton Industries) which has a 30 db gain and a 10% bandwidth. A. Bers[6] describes the performance of a 7-cavity hollow beam multicavity klystron with small-signal 30 db gain and 8.75% (power out/power in)-bandwidth. These klystrons have drift spaces between the cavities and no electromagnetic coupling between them.

Our computer program does, in fact, describe tubes in the above performance range if we insert a drift space between the optimized output cavity and its neighbor. The computations summarized below indicate that drift spaces between the other cavities are not required for good gain and bandwidth, although they undoubtedly help to optimize the performance, but an output cavity of low Q and high R_{sh} is indispensable. Electromagnetic coupling between the cavities can augment either the gain or the bandwidth with little or no reduction of the other quantity but too large a coupling can have a net detrimental effect. Stagger-tuning the cavities can be very beneficial if it is done correctly. The computations also indicate the desirability of a large (ω/ω_q)-ratio for good gain.

We conclude with a summary of the computations for various decoupled and coupled, synchronously-tuned and stagger-tuned model tubes used as bunchers. The bunchers analyzed were:

1a) a 5-cavity decoupled tube (m = 0), synchronously tuned.

1b) The same decoupled tube with the cavities stagger-tuned in 3 different ways.

2a) The same tube but coupled to m = -.04, synchronously tuned.

2b) The same tube of m = -.04 but stagger-tuned in the same three different ways.

---

[6] L. B. Anderson and A. Bers, "A Broadband Megawatt Hollow Beam Multicavity Klystron," lecture delivered at the 4th International Congress on Microwave Tubes, Scheveningen, Netherlands, September 3-7, 1962.

3a) The same tube but coupled now to $m = -.10$, synchronously tuned.

3b) The same tube of $m = -.10$ but stagger-tuned in the preceding three different ways. We studied these tubes both for $\theta_e = \frac{\pi}{2}$ and $\frac{3\pi}{4}$, with $C_B = 0.10$ and $\theta_q/\theta_e = 0.10$. Each model was externally loaded so that each cavity had a Q_L of 50 without the beam. Lastly, we considered

4) The 4-cavity skirtron tube, with the decoupled intermediate cavities synchronously-tuned, and also stagger-tuned in 3 different ways. $\theta_e = \pi/2$, $C_B = 0.20$, and $\theta_q/\theta_e = 0.11$. Each cavity had a Q_L of 25 in accord with the experimental parameters.[5]

We computed the kinetic voltage V_K and current leaving the last cavity, as well as the input resistance R_{in}, as functions of frequency. Assuming the output cavity is located 90 space-charge degrees beyond the last buncher cavity the beam current $Y_o V_K$ entering the output cavity gap is known, and the output power can be computed. For a study of the bandwidth it is sufficient to consider the relative transducer gain $G_{T,\,rel}$,

$$G_{T,\,rel} = \frac{|V_{K,\,out}|^2}{R_{in}} \frac{4R_g R_{in}}{(R_g + R_{in})^2} \quad \text{(refer to Eq. 30).} \tag{33}$$

The bandwidth of each model tube was optimized without sacrificing the maximum relative transducer gain by a suitable choice of R_g.

About half of the first group of tubes examined had bandwidths in the range 5-10%; the skirtron had a bandwidth exceeding 10%.

In order to estimate the <u>magnitude</u> of the maximum transducer gain associated with each of these models we let the parameters have the values

$$\left.\begin{aligned} V_o &= 85 \text{ kv} \\ I_o &= 100 \text{ amp} \\ \text{Perveance} &= 4 \times 10^{-6} \end{aligned}\right\} \tag{34}$$

$$\left.\begin{aligned} G_L &\cong G_{shunt} \text{ of output cavity} = I_o/V_o = 1.2 \times 10^{-3} \\ Q_L &\text{ of the output cavity} = 10 \end{aligned}\right\}$$

whereupon the maximum transducer gain was on the order of $1(\omega/\omega_q)^2$ for all of these tubes. Since $(\omega/\omega_q)^2 \sim 20$ db gain we see the need for as large an (ω/ω_q)-ratio as possible. As this ratio increases C_B of Eq. 16 also tends to increase, whereupon the transducer gain rises and the bandwidth can be maintained, perhaps with a readjustment of R_g.

Table 1

Equations for the Stagger-tuned Beam Amplifier

$$a_{11}\,\phi(1) + \frac{1}{2}\,\rho_2\, m_{21}\,\phi(2) - jDI_G = 0$$

$$a_{nn}\,\phi(n) + \frac{1}{2}\,\rho_{n-1}\, m_{n-1,n}\,\phi(n-1) + \frac{1}{2}\,\rho_{n+1}\, m_{n+1,n}\,\phi(n+1) + f V_K(n) + g I_b(n) = 0$$

$$a\,V_K(n) + c\,I_b(n) + b\,\phi(n) - V_K(n+1) = 0$$

$$c\,V_K(n) + a\,I_b(n) + d\,\phi(n) - I_b(n+1) = 0$$

$$a_{NN}\,\phi(N) + \frac{1}{2}\,\rho_{N-1}\, m_{N-1,N}\,\phi(N-1) + f\,V_K(N) + g\,I_b(N) = 0$$

in which these abbreviations have been introduced.

$$a_{nn} = \rho_n^{\,2} - K^2 + \rho_n\, m_{nn} + q + j\,Y_{Ln}$$

$$q = -K\,|e_z|\left[jS_e\left\{1 - \epsilon^{-j\theta_e}\left(\cos\theta_q + j\frac{\theta_e}{\theta_q}\sin\theta_q\right)\right\}\right.$$

$$\left. + S_q\left\{+\epsilon^{-j\theta_e}\left(\sin\theta_q - j\frac{\theta_e}{\theta_q}\cos\theta_q\right) + j\frac{\theta_e}{\theta_q}\right\} + 1\right]$$

$$f = K\left[\left(\cos\theta_q + j\frac{\theta_e}{\theta_q}\sin\theta_q\right)\epsilon^{-j\theta_e} - 1\right]$$

$$g = jK\left[\left(\sin\theta_q - j\frac{\theta_e}{\theta_q}\cos\theta_q\right)\epsilon^{-j\theta_e} + j\theta_e/\theta_q\right]$$

$$a = \cos\theta_q\,\epsilon^{-j\theta_e}$$

$$b = |\bar{e}_z|\left[-jS_e + jS_e\cos\theta_q\,\epsilon^{-j\theta_e} - S_q\sin\theta_q\,\epsilon^{-j\theta_e}\right]$$

$$c = j\sin\theta_q\,\epsilon^{-j\theta_e}$$

$$d = |\bar{e}_z|\left[-S_e\sin\theta_q\,\epsilon^{-j\theta_e} + jS_q\cos\theta_q\,\epsilon^{-j\theta_e} - jS_q\right]$$

$$S_e = \theta_e/(\theta_e^2 - \theta_q^2), \quad S_q = \theta_q/(\theta_e^2 - \theta_q^2)$$

$$K = -\frac{S_q \theta_e^2}{|e_z|} C_B^2, \quad C_B^2 \text{ given by Eq. 16.}$$

Table 2

Response of the Synchronously-tuned, Uncoupled 10-cavity Amplifier
$m = 0, \quad C_B = .028, \quad Y_{LN} = .02 + j0 \quad (Q_L = 50)$

κ (normalized frequency)+	G (power gain)	Z_{in} (ohms)
.9960	18	1.0 + j60.5
.9965	24	1.3 + j69.2
.9970	34	1.7 + j80.9
.9975	54	2.5 + j97.2
.9980	100	3.9 + j122
.9985	246	7.0 + j163
.9990	1.1×10^3	16.1 + j247
.9930	5.7×10^3	33.6 + j356
.9995	3.6×10^4	67.8 + j503
.9997	1.0×10^6	199 + j846
1.0000	2.1×10^7	3,050 - j1507

Table 3

Response of the Synchronously-tuned, Uncoupled 10-cavity Amplifier. $m = 0, \quad C_B = .0707, \quad Y_{LN} = .02 + j0$

κ	G	Z_{in}
.9930	2.5×10^3	2.0 + j35
.9950	1.2×10^4	3.9 + j50
.9960	3.7×10^4	6.2 + j62
.9965	7.7×10^4	8.2 + j72
.9970	1.9×10^5	11.3 + j84
.9975	5.9×10^5	16.6 + j101
.9980	2.7×10^6	26.6 + j127
.9985	2.3×10^7	48.8 + j169
.9990	5.9×10^8	113 + j242
1.0000	1.2×10^8	508 - j251

+ $\kappa = 1$ corresponds to operating frequency at the resonant frequency of each cavity.

Table 4

Response of the Synchronously-tuned, Uncoupled 10-cavity Amplifier

$m = 0, \quad C_B = .10, \quad Y_{LN} = .02 + j0$

κ	G	Z_{in}
.9930	1.2×10^5	4.1 + j36
.9950	1.0×10^6	8.3 + j51
.9960	4.7×10^6	13.3 + j64
.9965	1.2×10^7	17.6 + j73
.9970	4.1×10^7	24.4 + j84
.9975	1.7×10^8	35.8 + j100
.9980	1.1×10^9	56.7 + j121
.9985	1.1×10^{10}	98.9 + j147
.9990	1.3×10^{11}	188. + j155
.9995	2.0×10^{11}	308 + j51
1.0000	2.2×10^8	254 - j126

Table 5

Response of the Synchronously-tuned 10-cavity Amplifier with $m = -0.01$ and $C_B = .0285$. Output cavity is matched to the growing wave at the $3\pi/4$ "cold" circuit phase shift frequency.

κ^+	G^{++}	Z_{in}
.9968	1400	31.4 + j638
.9971	244	21.4 - j235
.9974	95	14.7 - j108
.9980	94	19.6 - j32.6
.9985	153	87.3 - j1.5

$^+\kappa = 1$ corresponds to the open-circuit mode resonant frequency which, in this synchronously-tuned chain, is the π-cutoff frequency.

$^{++}$Negative gain means negative output power, $R_{in} < 0$.

Table 5, Continued

κ	G	Z_{in}
.9989	243	118 + j0.2
.9990	407	202 + j62.2
.99906	889	540 + j 187
.99908	1611	1204 + j58.4
.99909	2801	1661 - j954
.99911	-5166	-252 - j1039
.99912	-2083	-282 - j683
.99916	-587	-158 - j289
.99920	-329	-99.2 - j196
.99950	-67	-18.8 - j82.4

Table 6

Response of the Tube of Table 5 but for $C_B = .10$

κ	G	Z_{in}
.9968	-229	-21.8 - j41.0
.9980	-440	-18.6 - j37.2
.99820	-1287	-19. 7 - j37. 5
.99832	-4176	-21.1 - j39.0
.99837	-8207	-21. 8 - j41.0
.99840	-13, 170	-21.7 - j43. 1
.99842	-18, 440	-20.8 - j45.0
.99845	-29,810	-17.5 - j47.1
.99848	-39, 340	-13.2 - j46.2
.99850	-38, 280	-11.6 - j44.3
.99860	-11, 360	-12.2 - j38.3
.9988	-2, 442	-14.2 - j37. 0
.9992	-575	-14.1 - j37.3

Table 7

Response of the Tube of Table 5 but for $m = -.04$, $C_B = .0707$

κ	G	Z_{in}
.983	23.9	3.6 - j9.3
.986	-114	-12.5 + j30.3
.988	-726	-3.7 - j55.6
.990	205	3.0 - j19.6
.993	334	15.3 + j0.3
.995	448	9.0 - j6.4
.996	-1374	-4.8 + j7.3
.998	-59	-7.3 - j18.0
1.000	-18	-5.4 - j13.2

Table 8

Response of the Tube of Table 5 but for $m = -.04$, $C_B = .10$

κ	G	Z_{in}
.983	-152	-2.7 - j3.3
.986	-58	-21.6 - j15.1
.988	-240	-5.4 - j20.6
.990	-1869	-0.8 - j12.7
.992	-2284	-2.3 - j 3.0
.993	-5014	-10.0 + j16.7
.994	+3016	11.3 - j20.6
.995	-14, 300	-0.5 - j7.7
.996	-473	-8.0 - j7.4
.998	-105	-6.6 - j13.7
1.000	-28	-4.3 - j12.6

Table 11

Response of the Stagger-tuned, 5-cavity Tube with the Parameters θ_e = 2.36, θ_q = 0.40, C_B = .10, m = 0. The output load Y_{Ln} = .02 + j 0, for a loaded Q_L = 50. The normalized resonant frequencies $\rho_1, \ldots, \rho_5$ are 1.0, 1.003, 1.0, .993, 1.0.

$\mathcal{K}$	G	Z_{in}
.990	442	4.1 + j 25.1
.992	1130	6.5 + j 31.4
.994	333	11.8 + j 41.5
.9955	50	21.3 + j 53.8
.997	19	46.3 + j 71.7
.998	120	87.5 + j 78.2
.999	386	148.9 + j 35.4
1.000	417	101.1 - j 75.2
1.002	127	39.4 - j 68.2
1.005	3	9.1 - j 36.7

Table 12

Response of the 5-cavity Tube of Table 11 but with the Resonant Frequencies 0.997, .994, 1.000, 1.006, 1.003.

$\mathcal{K}$	G	Z_{in}
.988	108	5.1 + j 28.0
.990	230	8.6 + j 35.9
.992	646	17.3 + j 49.2
.994	718	46.6 + j 71.8
.9955	166	119.5 + j 67.2
.997	16	134.0 - j 56.0
.998	27	73.2 - j 78.5
.999	143	39.5 - j 68.2
1.000	192	18.8 - j 51.1
1.002	90	10.7 - j 39.7
1.003	34	6.9 - j 32.1
1.005	1.4	4.2 - j 25.5

Table 13

Response of the 10-cavity Tube of Table 11 but with $m = -0.01$ and the Output Cavity Matched to the $3\pi/4$-phase-shift frequency. The normalized resonant frequencies are .996, .9965, .9970, .9975, .9980, .9985, .9990, .9995, 1.000, 1.000.

κ^+	G	Z_{in}
.9960	-262	-5.0 - j 30.4
.9968	-736	-3.7 - j 29.0
.9976	-459	-2.4 - j 27.4
.9984	-1033	-1.5 - j 25.7
.9992	-1270	-0.8 - j 24.1
1.0000	-955	-0.3 - j 22.6

Table 14

Response of the Tube of Table 13 but with the Resonant Frequencies .996, .9965, .997, .9975, .998, .9985, 1.000, 1.000, .9995, .9990.

κ	G	Z_{in}
.9960	-1420	-5.1 - j 30.3
.9964	-3648	-4.5 - j 29.9
.9968	-2711	-3.6 - j 29.2
.9972	0	-2.9 - j 27.9
.9976	-177	-2.4 - j 27.3
.9980	-16	-1.9 - j 26.5
.9984	-42	-1.5 - j 25.7
.9988	-117	-1.1 - j 24.9
.9992	-187	-0.8 - 24.1
.9996	-238	-0.5 - j 23.3
1.000	-288	-0.3 - j 22.6

$^+\kappa = 1$ corresponds to the open-circuit mode resonant frequency of the last cavity. This would be the π-cutoff frequency in an infinite chain of such cavities.